Indonesian Review of Physics (IRiP)
Vol.4, No.2, December 2021, pp. 1 - 7
p-ISSN: 2621-3761 | e-ISSN: 2621-2889
DOI: 10.12928/irip.v4i2.4920

Synthesis of Calcium Phosphate from Cockle Shell Loaded by Silver Nanoparticle and Its Antibacterial Activity Evaluation

Yuant Tiandho[1], Rahmad Lingga[2], Evi.J[3], Rifqi Almusawi Rafsanjani[4], and Fitri Afriani[5]*
[1,3,5] Department of Physics, Universitas Bangka Belitung, Indonesia
[2] Department of Biology, Universitas Bangka Belitung, Indonesia
[4] Department of Physics, Universitas Indonesia, Indonesia
Email: fitri-afriani@ubb.ac.id

Article Info

Article History
Received: Sept 25, 2021
Revised: Dec 15, 2021
Accepted: Dec 27, 2021

Keywords:
Calcium Phosphate
Silver Nanoparticles
Antibacterial
Green-Synthesis

ABSTRACT

This study aimed to synthesize calcium phosphate loaded with silver nanoparticles and evaluate its antibacterial activity. We used cockle shells waste as raw material to prepare calcium phosphate. X-ray diffraction analysis showed that the constituent phases of calcium phosphate consist of hydroxyapatite (HA) and β-tricalcium phosphate (β-TCP). The incorporation process of silver nanoparticles on calcium phosphate was carried out in colloidal silver nanoparticles via the green-synthesis method using Citrus x microcarpa Bunge peel extract. The presence of colloidal silver nanoparticles through the green synthesis method was identified using UV-Vis spectrophotometer by the peak of the absorption band that occurred at 468 nm. The incorporation of silver nanoparticles into calcium phosphate did not significantly change the crystalline properties of HA and β-TCP. Evaluation of the antibacterial activity showed the silver nanoparticles had a strong antibacterial effect against Staphylococcus aureus, which also occurs in calcium phosphate loaded by silver nanoparticles. After being incorporated with silver nanoparticles, Calcium phosphate generally has no antibacterial effect. After being incorporated with silver nanoparticles, an inhibition zone with a diameter of about 9.8 mm can form. These results indicated that the method proposed in this study could be an alternative for developing calcium phosphate, which requires self-sterilization properties.

To cite this article:
Y. Tiandho, R. Lingga, E. Evi.J, R. A. Rafsanjani, and F. Afriani, "Synthesis of Calcium Phosphate from Cockle Shell Loaded by Silver Nanoparticle and Its Antibacterial Activity Evaluation," *Indones. Rev. Phys.*, vol. 4, no. 2, pp. 1–7, 2021, doi: 10.12928/irip.v4i2.4920.

I. Introduction

The calcium phosphate ceramic family is a widely used material for biomedical and tissue engineering purposes [1]. Various types of calcium phosphate have good biocompatibility properties and do not show toxic effects for humans. Among various types of calcium phosphate ceramics, hydroxyapatite (HA) and β-tricalcium phosphate (β-TCP) are often used as bone substitution materials, dentistry, and orthopedics [2][3]. It is because both materials are biocompatible and biodegradable [4].

One novel application of calcium phosphate ceramics is used as a mask filtration material [5]. In addition to being biocompatible, the porous calcium phosphate has superior air filtration performance [6]. However, the use of calcium phosphate as a mask filtration medium and in orthopedics is often constrained by its antibacterial activity. Calcium phosphate is known to be unable to form a zone of inhibition in bacterial culture and has no antibacterial effect.

One potential solution to raise the antibacterial effect in calcium phosphate is through substitute silver nanoparticles in its structure. Silver nanoparticles have high antibacterial activity and are biocompatible [7][8].

This work synthesizes calcium phosphate-loaded silver nanoparticles mediated by *Citrus x macrocarpa* Bunge (*C. x macrocarpa* Bunge) peel extract. We modified the green-synthesis method that utilizes biological objects such as plant extracts to substitute silver

nanoparticles into calcium phosphate. It aims to minimize the use of chemical compounds that are toxic and not environmentally friendly. We used the *C. x microcarpa* Bunge peel extract because of its phytochemical compounds, which can act as a reducing agent and capping agent in synthesizing nanoparticles and its abundance in the Bangka Belitung Islands. The fruit of *C. x microcarpa* Bunge is used by local people to source a sour flavor in various foods. In addition, in preparing calcium phosphate, we use cockle *Anadara granosa* (*A. granosa*) shells as the raw material. Cockle shells contain high amounts of calcium carbonate to be used to synthesize calcium phosphate ceramics [9]. The utilization of raw materials derived from natural materials avoids toxic contaminants and maintains their sustainability.

II. Theory

Calcium phosphate is a group of minerals that contain calcium together with orthophosphate (PO_4^3), metaphosphate (PO_3^-), or pyrophosphate ($P_2O_7^{4-}$), and sometimes with hydrogen ions or hydroxide ions. Two phases of calcium phosphate, which are very prominently applied in tissue engineering, are HA ($Ca_{10}(PO_4)_6(OH)_2$) and β-TCP ($Ca_3(PO_4)_2$). This is because both are biocompatible, non-toxic, and biodegradable [1][10]. The crystalline properties of HA and β-TCP are presented in Table 1 and Table 2.

HA and β-TCP can be synthesized by reacting calcium materials, for example, CaO, with a phosphate source such as H_3PO_4 or $(NH_4)_2HPO_4$. Therefore, there have been many studies on the synthesis of HA and TCP using natural materials rich in calcium, such as eggshells [11], bovine bones [12], and fish bones [13], in recent years [14].

Silver nanoparticles are widely known materials to have vigorous antibacterial activity [15]. In summary, the mechanism of antibacterial activity of silver nanoparticles can occur based on the following steps: (i) the presence of silver nanoparticles damages the cell walls and cytoplasmic membranes of bacteria; (ii) ribosome denaturation occurs and inhibits protein synthesis; (iii) interfere with bacterial ATP production because silver ions entering the bacterial system will inhibit the respiratory system; (iv) silver nanoparticle ions and reactive oxygen bind to DNA so that cell replication and multiplication processes cannot occur; (v) the membrane denaturation process occurs, and (vi) perforation of the bacterial membrane occurred as indicated by the ability of silver nanoparticles to pass through the cytoplasmic membrane and destroy cell organelles [16].

There are many methods to synthesize silver nanoparticles. However, considering that silver nanoparticles will be applied in the biomedical field, the main problem in the synthesis process is to avoid using toxic chemical compounds. Therefore, the green-synthesis method using natural sources such as plant extracts is proposed as a promising alternative solution [17]. Various phytochemical compounds from plant extracts containing phenolic compounds can reduce particle size. This is because phenolic compounds have hydroxyl aromatic ring groups that can act as ligands to prevent agglomeration during the synthesis process [18].

Table 1. Crystalline properties of HA [19].

Space Group	:	**P 63/M**		
Lattice Parameter	:			
a (Å)	:	9.41844		
b (Å)	:	9.41844		
c (Å)	:	6.88374		
Atomic coordinates		*x*	*y*	*z*
Ca (1)	:	0.3333	0.6667	0.0016
Ca (2)	:	0.2460	0.9923	0.2500
P	:	0.3980	0.3680	0.2500
O (1)	:	0.3275	0.4841	0.2500
O (2)	:	0.5869	0.4649	0.2500
O (3)	:	0.3436	0.2580	0.0705
O	:	0.0000	0.0000	0.1975
H	:	0.0000	0.0000	0.0540

Table 2. Crystalline properties of β-TCP [20].

Space Group	:	**R 3 C**		
Lattice Parameter	:			
a (Å)	:	10.417		
b (Å)	:	10.417		
c (Å)	:	37.329		
Atomic coordinates		*x*	*y*	*z*
Ca(1)	:	-0.2766	-0.1421	0.1658
Ca(2)	:	-0.3836	-0.1775	-0.0336
Ca(3)	:	-0.2721	-0.1482	0.0606
Ca(4)	:	0.0000	0.0000	-0.0850
Ca(5)	:	0.0000	0.0000	-0.2658
P(1)	:	0.0000	0.0000	0.0000
P(2)	:	-0.3109	-0.1365	-0.1320
P(3)	:	-0.3465	-0.1537	-0.2333
O(1)	:	-0.2736	-0.0900	-0.0926
O(2)	:	-0.2302	-0.2171	-0.1446
O(3)	:	-0.2735	0.0053	-0.1523
O(4)	:	-0.4777	-0.2392	-0.1378
O(5)	:	-0.4031	-0.0489	-0.2211
O(6)	:	-0.4246	-0.3056	-0.2152
O(7)	:	0.1814	-0.0805	-0.2233
O(8)	:	-0.3696	-0.1748	-0.2735
O(9)	:	0.0070	-0.1366	-0.0136
O(10)	:	0.0000	0.0000	0.0400

III. Method

Preparation of Calcium Phosphate from Cockle Shells

The cockle shells (*A. granosa*) used in this study were collected from the Pangkalpinang City market, Bangka Belitung Islands, Indonesia. The cockle shells were washed and dried in the sun to eliminate macro dirts. The cockle shells were calcined at 1000 °C to decompose calcium carbonate compounds as given in the following reaction [21]:

$$CaCO_3 \rightarrow CaO+CO_2 \quad (1)$$

p-ISSN: 2621-3761
e-ISSN: 2621-2889

Afterward, calcined cockle shells were dissolved into 100 mL of distilled water. As a phosphate source, we added H_3PO_4 solution at a Ca/P ratio of 1.5. Precipitation was carried out using a magnetic stirrer at a temperature of 50 °C for 2 hours. The residue was sintered at 1000°C for 7 hours, thus considered a stock calcium phosphate for synthesis.

Preparation of C. x microcarpa Bunge Peel Extract

We used *C. x microcarpa* Bunge fruit waste from Bangka Regency, Bangka Belitung Islands, Indonesia. We grounded the peel using a blender to obtain a coarse powder to facilitate the extraction process, as shown in Figure 1. Afterward, we used the maceration method to produce the extract by mixing two gr of peel powder with five mL distilled water as a solvent. The extract preparation process was carried out using a magnetic stirrer at a temperature of 100° ℃. The extract was filtered and stored at 4℃ for further use.

Synthesis of calcium phosphate loaded with silver nanoparticles

About 12 grams of $AgNO_3$ was dissolved in 400 ml of distilled water and stirred for 30 minutes. Afterward, 100 ml of *C. x microcarpa* Bunge extract was added and stirred for 48 hours. As an accelerator, we added NaOH until pH = 7 was reached. The synthesis of calcium phosphate loaded with silver nanoparticles was carried out by adding calcium phosphate to 100 ml of silver nanoparticles in the extract and stirring for one hour. In this study, we varied the concentration of calcium phosphate by 3 grams (CP3/Ag) and 5 grams (CP5/Ag). The powder was filtered and dried using an oven at 110℃. Schematically, the calcium phosphate synthesis route containing silver nanoparticles in this study is shown in Figure 2.

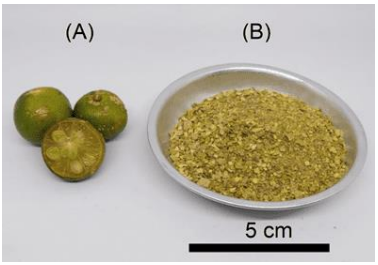

Figure 1. (a) *C. x microcarpa* Bunge fruit and (b) the grounded peels

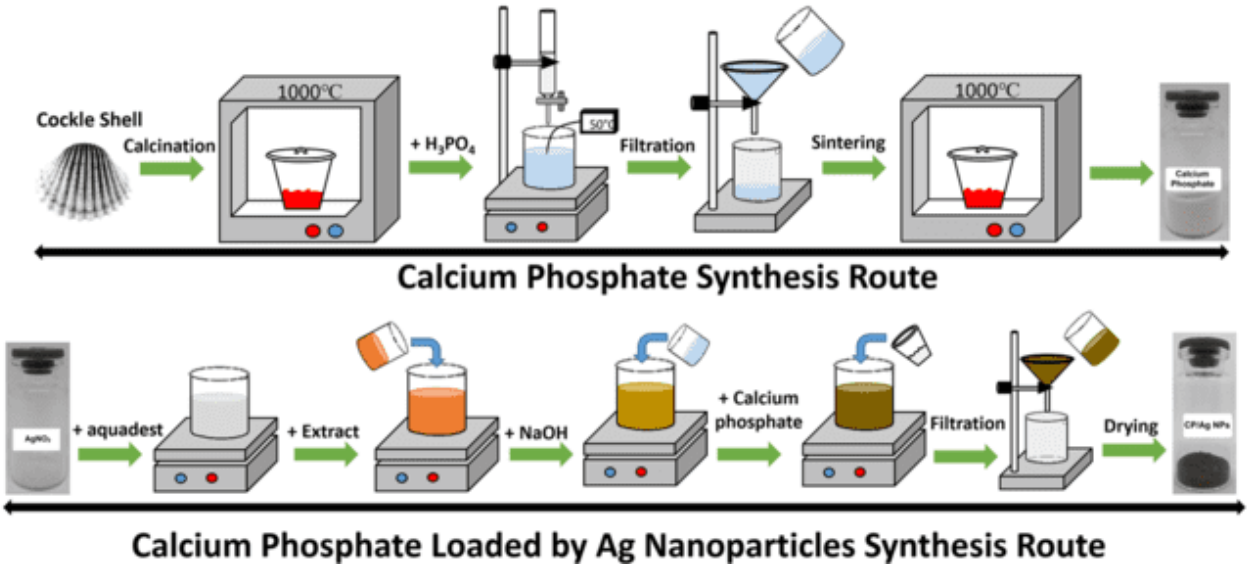

Figure 2. Schematic diagram of calcium phosphate synthesis (top) and calcium phosphate loaded silver nanoparticles synthesis (bottom) routes

Material Characterization and Antibacterial Activity

To investigate the crystalline properties of the synthesized calcium phosphate, in both pure calcium phosphate and calcium phosphate loaded by silver nanoparticles, we used X-ray diffraction (XRD). We analyzed the XRD data using the Rietveld method. The presence of colloidal silver nanoparticles formed in the green synthesis was indicated by the absorption band using a UV-Vis spectrophotometer in the range of 200 nm – 900 nm. The absorption peak that appears is related to the surface plasmon resonance of the silver nanoparticles.

p-ISSN: 2621-3761
e-ISSN: 2621-2889

Antibacterial activity was conducted against *Staphylococcus aureus* (*S. aureus*) bacteria by disc paper diffusion method. The bacterial growth medium we used in this study was nutrient agar (NA), and microbial inoculation was done by streaking the bacterial suspension on the NA medium. Furthermore, the disc paper that had been dipped in a mixture of calcium phosphate loaded with silver nanoparticles was placed on NA medium and incubated for 24 hours at 37°C. The experiment was repeated three times, and the antibacterial activity was indicated by the average diameter of the inhibition zone.

IV. Results and Discussion

Figure 3 shows the XRD pattern of the calcium phosphate synthesized in this work. After the refinement process, it is known that the types of calcium phosphate formed are HA and β-TCP. The goodness of fit coefficient value ($\chi 2$) of 0.205 indicates that the refinement has good quality. The three highest peaks associated with HA are indicated by peaks 52.97°, 30.97°, and 31.09°, and these peaks correspond to orientations 0 4 14, 0 2 10, and 2 1 7. Crystal structure of the synthesized HA is hexagonal with space group P 63/M and has cell parameters: $a = b =$ 9.3893 Å and c = 6.8839 Å. The three highest peaks associated with β-TCP are at positions 31.05°, 34.39°, and 27.82° and correspond to orientations 0 2 10, 2 2 0, and 2 1 4. The crystal structure of the synthesized β-TCP is trigonal with space group R 3 C. The cell parameters of β-TCP are $a = b$ = 10.431Å and c = 37.3858 Å. The cell volumes of HA and β-TCP were 525.58 $Å^3$ and 3522.81 $Å^3$, respectively. Refinement calculations show that the molar percentages of HA and β-TCP are 12.98% and 87.02%, respectively. It indicates that calcium phosphate synthesized is dominated by β-TCP. It occurs because the Ca/P ratio of H_3PO_4 used is close to the Ca/P ratio of β-TCP. The diffraction pattern of β-TCP synthesized in this study is similar to other studies such as Afriani et al. (2015), who synthesized TCP from eggshell [11], and Kang et al. (2017), who synthesized β-TCP from abalone shell [22]. By substituting cell parameter data and atomic coordinates of HA and β-TCP, the crystal structure of both phases is presented in Figure 4.

Figure 5 shows the color change of the *C. x microcarpa* Bunge extract after $AgNO_3$ was added from initially orange to black. The color change indicates that silver nanoparticles have started to form in the mixture. This transformation can also be observed through the absorbance band of the UV-Vis spectrophotometer in Figure 6. The absorbance peak of the extract of *C. x microcarpa* Bunge occurred at wavelengths of 276 nm and 320 nm. The absorbance peak is related to the characteristics of the abundant citric acid in this plant [23]. After mixing with $AgNO_3$, an absorbance peak was formed at a wavelength of 468 nm. The absorbance peak indicates that silver nanoparticles have been formed in the mixture. This is because noble metals have unique optical properties due to their surface plasmon resonance (SPR) properties. SPR is a collective oscillation of the conduction electrons under resonance conditions with the wavelength of the illuminating light. The type, size, and shape of the nanoparticles affect the spectral position of the plasmon band absorption. In various studies, it is known that SPR of silver nanoparticles occurs at a wavelength of 400-500 nm [24].

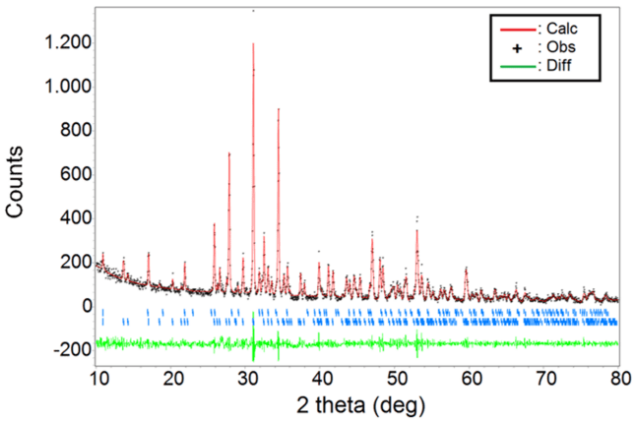

Figure 3. XRD pattern of calcium phosphate synthesized from cockle shell waste. The + symbol indicates the experimental data (obs), and a solid line indicates the calculation (calc) of the refinement. The lower trace is the difference between experiment and calculation (diff). The vertical lines mark the position of the calculated Bragg peaks for an HA and β-TCP, respectively.

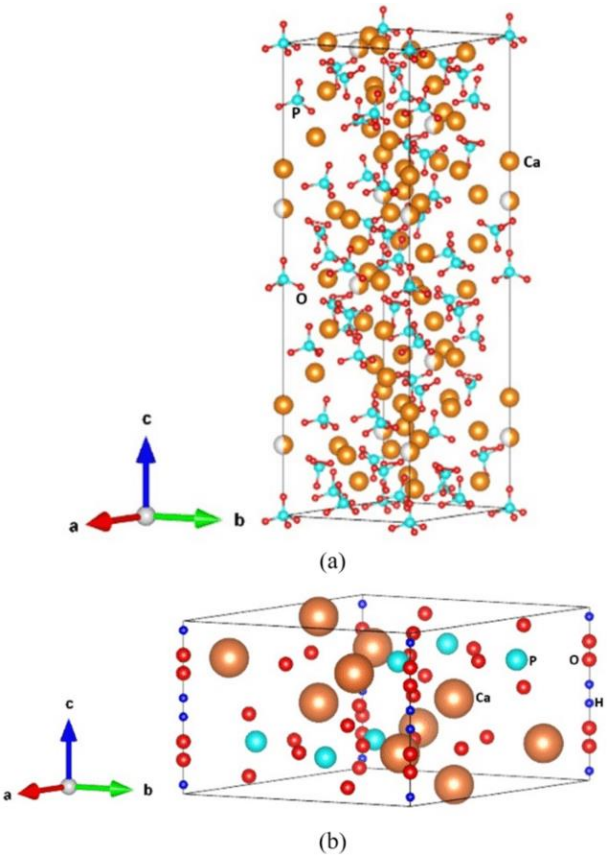

Figure 4. Structure of: (a) β-TCP and (b) HA; color code: Ca atoms in brown, P atoms in turquoise, O atoms in red and H atoms in blue. Image created with VESTA [25].

p-ISSN: 2621-3761
e-ISSN: 2621-2889

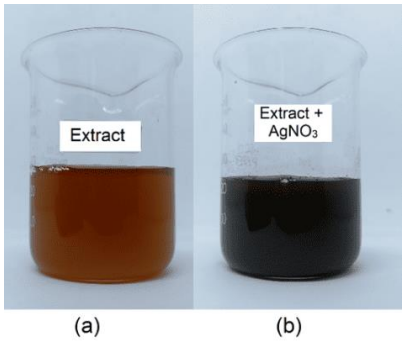

Figure 5. Visual changes in the extract: (a) before and (b) after mixed with $AgNO_3$

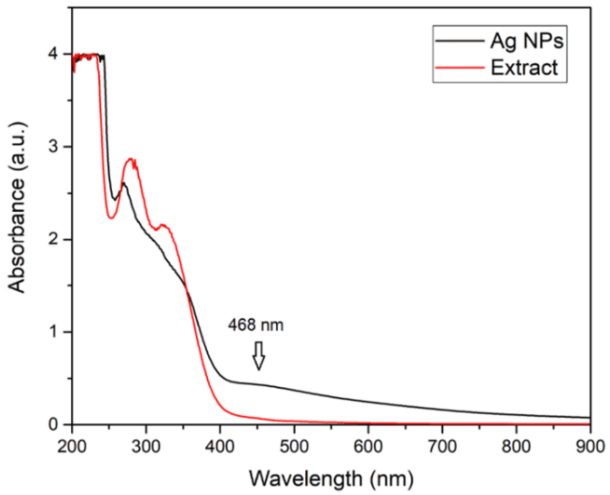

Figure 6. UV-Visible spectra of *C. x microcarpa* Bunge skin extract and silver nanoparticles synthesized by green synthesis method

Figure 7 presents the refinement results of the XRD pattern of calcium phosphate loaded with silver nanoparticles. The XRD pattern in Figure 7(a) is the XRD pattern for the CP3/Ag, and the XRD pattern in Figure 7(b) is the XRD pattern for the CP5/Ag. The refinement for the XRD pattern belonging to CP3/Ag has a goodness of fit coefficient value (χ^2) of 0.457. The three compounds correlated with the XRD pattern were HA, β-TCP, and silver nanoparticles. After loading the silver nanoparticles, there was no significant change in HA and β-TCP type of crystal structure, each still in the space group P 63/M and R 3 C. The cell parameters of HA were $a = b = 9.3394$ Å and $c = 6.888$ Å while the cell parameters of β-TCP are $a = b = 10.4818$ Å and $c = 37.4468$. The cell volumes of HA and β-TCP were 520.3 Å^3 and 3563.01 Å^3, respectively. Compared with the initial conditions, the volume of HA cells slightly decreased while the volume of β-TCP cells expanded slightly. The cell parameters of silver nanoparticles in CP3/Ag are $a = b = c = 4.0973$ Å with a cell volume of 68.78 Å^3. Based on the calculations, the molar percentages of HA, β-TCP, and silver nanoparticles in CP3/Ag are 12.53%, 85.81%, and 1.66%, respectively. Through refinement, as shown in Figure 7(b), which has a goodness of fit coefficient (χ^2) of 0.867, it is also known that the XRD pattern of CP5/Ag is related to the HA, β-TCP, and silver nanoparticles phases. The three phases have the same space group as in CP3/Ag, namely HA in P 63/M, β-TCP in R 3 C, and silver nanoparticles in F M 3 M. Cell parameters of HA, β-TCP, and silver nanoparticles are $a = b = 9.3387$ Å and $c = 6.8935$ Å; $a = b = 10.4781$ Å and $c = 37.424$ Å, $a = b = c = 4.097$ Å, respectively. The cell volumes of the three phases are 520.64 Å^3, 3558.33 Å^3, and 68.75 Å^3. Through refinement calculations, the molar percentages of the HA, β-TCP, and silver nanoparticles phases were 12.55%, 85.79%, and 1.66%, respectively. There was no significant difference between the molar percentages of CP3/Ag and CP5/Ag. It indicates that adding 3 grams of calcium phosphate and 5 grams to 100 ml of prepared colloidal silver nanoparticles can contain the same amount of silver nanoparticles. It occurs because the amount of colloidal silver nanoparticles is still above the loading capacity of calcium phosphate.

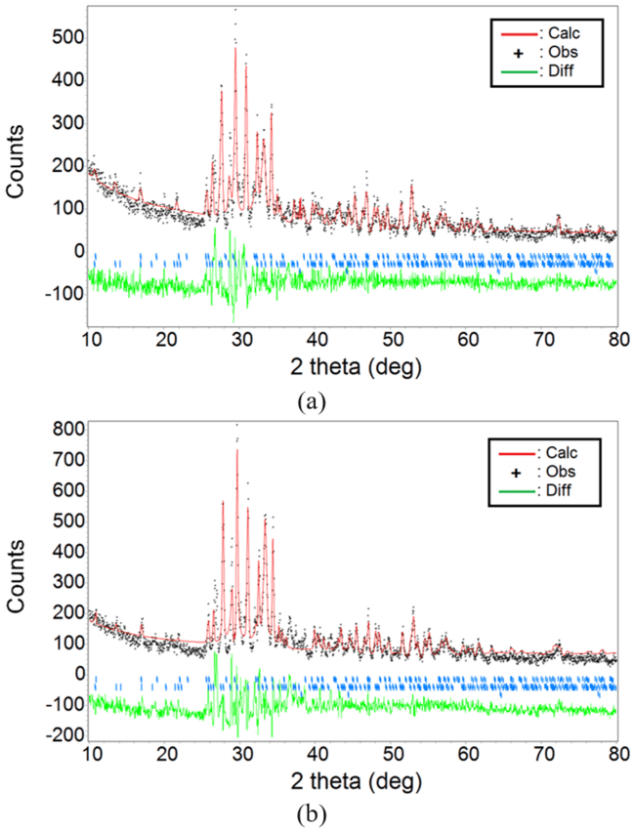

Figure 7. XRD pattern of calcium phosphate loaded by silver nanoparticles: (a) TCP3/Ag and (b) TCP5/Ag. The + symbol indicates the experimental data (obs), and a solid line indicates the calculation (calc) of the refinement. The lower trace is the difference between experiment and calculation (diff). The vertical lines mark the position of the calculated Bragg peaks for an HA, β-TCP, and silver nanoparticles, respectively

Figure 8 shows the inhibition zone of calcium phosphate loaded with silver nanoparticles and pure silver nanoparticles. Based on these results, it appears that calcium phosphate loaded with silver nanoparticles has an inhibition zone indicating an antibacterial effect. The

p-ISSN: 2621-3761
e-ISSN: 2621-2889

inhibition zone of CP3/Ag and CP5/Ag was (9 ± 4) mm and (10 ± 3) mm, respectively. It appears that the two calcium phosphates loaded with silver nanoparticles have no significantly different inhibition zones. It can happen because, based on XRD analysis, the molar percentage of silver nanoparticles in calcium phosphate does not have a significant difference. As shown in Figure 8(c), the silver nanoparticles synthesized in this study had the widest inhibition zone with (22 ± 2) mm diameter. The high activity of silver nanoparticles is because silver nanoparticles, through the presence of Ag^+ ions, can damage the cell walls and membranes of *S. aureus* and then interact with S and P-containing compounds, inhibiting the process of respiration replication and inactivating proteins.

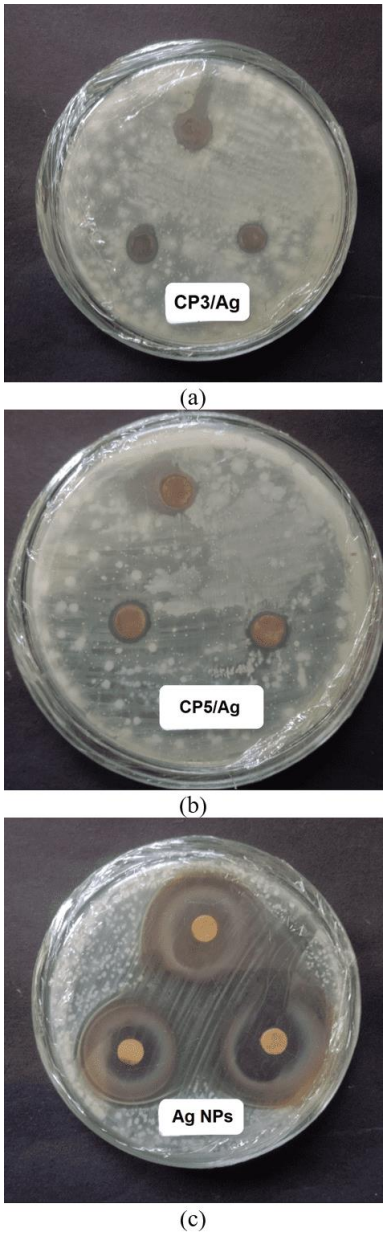

Figure 8. Inhibition zones of (a) CP3/Ag, (b) CP5/Ag, and silver nanoparticles against *S. Aureus*.

V. Conclusion

This study successfully synthesized calcium phosphate from cockle shell waste. We also incorporated silver nanoparticles into the calcium phosphate structure to obtain an antibacterial effect through the green synthesis method. XRD pattern analysis showed that the calcium phosphate produced was composed of two calcium phosphate phases, namely HA and β-TCP. The use of *C. x microcarpa* Bunge peel extract in green-synthesis of silver nanoparticles also showed satisfactory results. Through the UV-Vis absorption band pattern related to the surface plasmon frequency of silver nanoparticles, it has been indicated that colloidal silver nanoparticles can be formed through the green-synthesis method. The synthesized silver nanoparticles had a strong antibacterial effect against *S. aureus*. Therefore, investigations on the antibacterial activity of calcium phosphate loaded with silver nanoparticles also showed an antibacterial effect. Thus, the method offered in this research can be used in the future to develop calcium phosphate-based biocompatible materials that have self-sterilization properties.

VI. Acknowledgment

This research was funded by the Institute for Research and Community Services (LPPM) - Universitas Bangka Belitung through Hibah Penelitian Unggulan scheme in 2021 (No.: 17.29/UN50/PP/III/2021).

References

[1] N. Eliaz and N. Metoki, "Calcium Phosphate Bioceramics: A Review of Their History, Structure, Properties, Coating Technologies and Biomedical Applications," *Materials (Basel).*, vol. 10, no. 4, 2017, doi: 10.3390/ma10040334.

[2] D. Arcos and M. Vallet-regí, "Europe PMC Funders Group Substituted Hydroxyapatite Coatings of Bone Implants," vol. 8, no. 9, pp. 1781–1800, 2021, doi: 10.1039/C9TB02710F.

[3] Y. Cao, L. Xiao, Y. Cao, A. Nanda, C. Xu, and Q. Ye, "3D Printed β-TCP Scaffold with Sphingosine 1-Phosphate Coating Promotes Osteogenesis and Inhibits Inflammation," *Biochem. Biophys. Res. Commun.*, vol. 512, no. 4, pp. 889–895, 2019, doi: 10.1016/j.bbrc.2019.03.132.

[4] M. Taherimehr, R. Bagheri, and M. Taherimehr, "In-Vitro Evaluation of Thermoplastic Starch/Beta-Tricalcium Phosphate Nano-Biocomposite in Bone Tissue Engineering," *Ceram. Int.*, vol. 47, no. 11, pp. 15458–15463, 2021, doi: 10.1016/j.ceramint.2021.02.111.

[5] L. Zhao *et al.*, "Synthesis and Characterization of Silver-Incorporated Calcium Phosphate Antibacterial Nanocomposites for Mask Filtration Material," *Compos. Part B Eng.*, vol. 153, no. August, pp. 387–392, 2018, doi: 10.1016/j.compositesb.2018.09.004.

[6] S. Mukherjee, S. Kumar, R. K. Sahu, and S. Nayar, "PVA-Graphene-Hydroxyapatite Electrospun Fibres as Air-Filters," *Mater. Res. Express*, vol. 6, no. 12, p. 125366, Jan. 2020, doi: 10.1088/2053-1591/ab6ac9.

p-ISSN: 2621-3761
e-ISSN: 2621-2889

[7] Y. Q. Shen, Y. J. Zhu, F. F. Chen, Y. Y. Jiang, Z. C. Xiong, and F. Chen, "Antibacterial Gluey Silver-Calcium Phosphate Composites for Dentine Remineralization," *J. Mater. Chem. B*, vol. 6, no. 30, pp. 4985–4994, 2018, doi: 10.1039/C8TB00881G.

[8] M. N. Capela *et al.*, "Bioactivity and Antibacterial Activity Against E-Coli of Calcium-Phosphate-Based Glasses: Effect of Silver Content and Crystallinity," *Ceram. Int.*, vol. 43, no. 16, pp. 13800–13809, 2017, doi: 10.1016/j.ceramint.2017.07.100.

[9] F. Afriani, E. J, Z. Zaitun, and Y. Tiandho, "Improvement of Hardness of Hydroxyapatite by the Addition of Silica from Tin Tailings," *J. Eng. Sci. Res.*, vol. 2, no. 2, pp. 85–89, 2020, doi: 10.23960/jesr.v2i2.48.

[10] M. T. Islam, R. M. Felfel, E. A. Abou Neel, D. M. Grant, I. Ahmed, and K. M. Z. Hossain, "Bioactive Calcium Phosphate–Based Glasses and Ceramics and Their Biomedical Applications: A Review," *J. Tissue Eng.*, vol. 8, 2017, doi: 10.1177/2041731417719170.

[11] F. Afriani, K. Dahlan, S. Nikmatin, and O. Zuas, "Alginate Affecting the Characteristics of Porous Beta-TCP/Alginate Composite Scaffolds," *J. Optoelectron. Biomed. Mater.*, vol. 7, no. 3, pp. 67–76, 2015, [Online]. Available: https://chalcogen.ro/67_Afriani.pdf.

[12] D. G. Syarif, D. H. Prajitno, A. Kurniawan, M. B. Febrian, and R. Lesmana, "Hydrothermally Synthesis and Characterization of HAp and Zr-doped HAp Nanoparticles From Bovine Bone and Zircon for Photodynamic Therapy," *Process. Appl. Ceram.*, vol. 15, no. 2, pp. 146–153, 2021, doi: 10.2298/PAC2102146S.

[13] M. R. Hasan, N. S. Mohd Yasin M. S. Mohd Ghazali, and N. F. Mohtar, "Proximate and Morphological Characteristics of Nano Hydroxyapatite (Nano Hap) Extracted From Fish Bone," *J. Sustain. Sci. Manag.*, vol. 15, no. 8, pp. 9–21, 2020, doi: 10.46754/jssm.2020.12.002.

[14] F. Afriani, Siswoyo, R. Amelia, M. Hudatwi, Zaitun, and Y. Tiandho, "Hydroxyapatite From Natural Sources: Methods and Its Characteristics," *IOP Conf. Ser. Earth Environ. Sci.*, vol. 599, no. 1, pp. 0–7, 2020, doi: 10.1088/1755-1315/599/1/012055.

[15] C. G. A. Das *et al.*, "Antibacterial Activity of Silver Nanoparticles (Biosynthesis): A Short Review on Recent Advances," *Biocatal. Agric. Biotechnol.*, vol. 27, p. 101593, 2020, doi: 10.1016/j.bcab.2020.101593.

[16] I. X. Yin, J. Zhang, I. S. Zhao, M. L. Mei, Q. Li, and C. H. Chu, "The Antibacterial Mechanism of Silver Nanoparticles and Its Application in Dentistry," *Int. J. Nanomedicine*, vol. 15, pp. 2555–2562, 2020, doi: 10.2147/IJN.S246764.

[17] A. M. Awwad, N. M. Salem, M. M. Aqarbeh, and F. M. Abdulaziz, "Green Synthesis, Characterization of Silver Sulfide Nanoparticles and Antibacterial Activity Evaluation," *Chem. Int.*, vol. 6, no. 1, pp. 42–48, 2020, doi: 10.5281/zenodo.3243157.

[18] T. Ahmad, M. A. Bustam, M. Irfan, M. Moniruzzaman, H. M. A. Asghar, and S. Bhattacharjee, "Mechanistic Investigation of Phytochemicals Involved in Green Synthesis of Gold Nanoparticles Using Aqueous Elaeis Guineensis Leaves Extract: Role of Phenolic Compounds and Flavonoids," *Biotechnol. Appl. Biochem.*, vol. 66, no. 4, pp. 698–708, 2019, doi: 10.1002/bab.1787.

[19] D. Bazin *et al.*, "Diffraction Techniques and Vibrational Spectroscopy Opportunities to Characterise Bones," *Osteoporos. Int.*, vol. 20, no. 6, pp. 1065–1075, 2009, doi: 10.1007/s00198-009-0868-3.

[20] B. Dickens, L. W. Schroeder, and W. E. Brown, "Crystallographic Studies of the Role of Mg as A Stabilizing Impurity in β-Ca3(PO4)2. The Crystal Structure of Pure β-Ca3(PO4)2," *J. Solid State Chem.*, vol. 10, no. 3, pp. 232–248, 1974, doi: 10.1016/0022-4596(74)90030-9.

[21] F. Afriani, Mustari, and Y. Tiandho, "Pengaruh Lama Pemanasan terhadap Karakteristik Kristal Kalsium dari Limbah Cangkang Kerang [Effect of Heating Time on the Characteristics of Calcium Crystals from Shell Shell Waste]," *J. EduMatSains*, vol. 2, no. 2, pp. 189–200, 2018, doi: 10.33541/edumatsains.v2i2.606.

[22] K.-R. Kang *et al.*, "Synthesis and Characterization of β-Tricalcium Phosphate Derived From Haliotis sp. Shells," *Implant Dent.*, vol. 26, no. 3, pp. 378–387, Jun. 2017, doi: 10.1097/ID.0000000000000559.

[23] S. Mohan, Y. Singh, D. K. Verma, and S. H. Hasan, "Synthesis of CuO Nanoparticles Through Green Route Using Citrus Limon Juice and Its Application as Nanosorbent for Cr(VI) remediation: Process Optimization with RSM and ANN-GA Based Model," *Process Saf. Environ. Prot.*, vol. 96, pp. 156–166, 2015, doi: 10.1016/j.psep.2015.05.005.

[24] T. C. Prathna, N. Chandrasekaran, A. M. Raichur, and A. Mukherjee, "Biomimetic Synthesis of Silver Nanoparticles by Citrus Limon (Lemon) Aqueous Extract and Theoretical Prediction of Particle Size," *Colloids Surfaces B Biointerfaces*, vol. 82, no. 1, pp. 152–159, 2011, doi: 10.1016/j.colsurfb.2010.08.036.

[25] K. Momma and F. Izumi, "VESTA 3 for Three-Dimensional Visualization of Crystal, Volumetric and Morphology Data," *J. Appl. Crystallogr.*, vol. 44, no. 6, pp. 1272–1276, 2011, doi: 10.1107/S0021889811038970.

p-ISSN: 2621-3761
e-ISSN: 2621-2889